J. Fluid Mech. (1969), *vol.* 36, *part* 2, *pp.* 347–366
Printed in Great Britain

Numerical studies of the laminar boundary layer for Mach numbers up to 15

By HENRY A. FITZHUGH†
Department of Aeronautics, Imperial College, London University

(Received 25 June 1968)

A comprehensive set of exact solutions to the first-order boundary-layer equations has been computed using the finite difference computer programme of Sells, with and without wall cooling. The effects of Prandtl number, wall cooling and Mach number on separation point location were studied. Values of displacement thickness, skin friction coefficient and Stanton number are displayed graphically for the supersonic flow over a circular concave arc, for a subsonic cooled cylinder and for the case of a linearly retarded velocity distribution. The influence of pressure gradient on recovery factor was studied. Velocity and temperature profiles are shown for four cold wall cases. The exact computer results show the errors in many of the more approximate methods available for the case where $U_e = U_\infty(1 - X/L)$. The importance of second-order effects and the applicability of a first-order solution are discussed briefly.

1. Introduction

These numerical experiments were intended to be comprehensive and as many effects were studied as possible. Much more information is given than in previous exact solutions, including boundary-layer profiles and displacement thicknesses.

The computer solutions serve two purposes. They provide a standard against which the various approximate theories can be measured, and they indicate trends. Until now, very few exact solutions have been published for the compressible boundary-layer equations with wall cooling.

Sells' (1966) computer programme solves the first-order boundary-layer momentum, energy and continuity equations assuming only a perfect diatomic gas of constant Prandtl number flowing over a wall of constant temperature. The inviscid solution over the body in question is specified before calculation begins. Sells' method of solution of two coupled non-linear partial differential equations employs an implicit finite difference scheme and an estimation of the non-linear terms. The resulting non-homogeneous linear equations are solved by matrix inversion, the non-linear terms are re-evaluated and the process is repeated until the solution converges to within some pre-set limit. The programme then marches downstream utilizing the parabolic nature of the equations. Sells finds that results for skin friction are accurate to four significant figures, three

† Present address: Research Division, McDonnell Douglas Corporation, St Louis, Missouri, U.S.A.

near separation. The programme is capable of integrating close to separation and usually fails to converge at some point less than one step length from the extrapolated separation point. Occasionally the programme integrates one step length beyond separation, but errors in calculation using a reversed flow velocity profile are thought to be so great that convergence cannot be obtained any further downstream.

Stewartson (1964) states that the singular point in the boundary-layer should lie upstream of the separation point for a cold wall. The present calculations can tell us nothing about the singular point location because the step lengths used in the calculation are too large. It would appear that the programme passed the singular point on the occasions when it converged beyond separation.

The programme as published did not converge at Mach numbers above four and a great deal of time was spent trying to force convergence by numerical techniques less accurate than those originally employed. However, it was later realized that in the scaled variables used in the machine code, the scaled boundary-layer thickness decreases with increasing Mach number, which is the oppposite trend to the physical growth. It is necessary to specify η_i, the value of η where the boundary layer is assumed to asymptote to the free stream, as an input to the programme where η is the Dorodnitsyn normal co-ordinate $\int_0^Y \rho/\rho_\infty \, dY$ and (X, Y) are Cartesian co-ordinates. The programme then divides the boundary layer into a pre-specified number of steps (200 usually). For Mach numbers up to four, $\eta_i = 6$, but this had to be reduced progressively to 1 at $M = 10$ and 0·025 at $M = 22$. When the input parameters were adjusted accordingly, it was found that the original programme worked perfectly well at any Mach number up to the limit tested, i.e. $M = 22$.

2. Flow fields studied

By far the most common, relevant problem reported in the literature is the growth of a laminar boundary layer in a linearly retarded velocity field, i.e. $U_e = U_\infty(1 - X/L)$ where U is the velocity in the streamwise direction, L is the length of the body and the subscripts e and ∞ denote the edge of the boundary layer and free-stream conditions, respectively. Morduchow (1965) has given an excellent summary of the results of such calculations available before 1965; a few more have appeared since then. The method of Sells has now been used to solve the same problem in order to compare the results with those reported previously.

The body shapes that generate a linearly retarded velocity field are shown in figure 1, assuming Prandtl–Meyer compression.

In the solution of the linearly retarded velocity distribution the body contour varies with Mach number. Therefore in order to see trends more clearly the boundary-layer growth over a circular arc of unit-semi-circumference was calculated. The external (adverse) pressure gradient was determined assuming isentropic Prandtl–Meyer compression.

The cases studied are listed in tables 2–4. The properties calculated were

$(\delta^*/L)\sqrt{R_X}$, $C_f\sqrt{R_X}$ and $S_t\sqrt{R_X}$ from the leading edge to the separation point where δ^* is the boundary-layer displacement thickness, R_X is the Reynolds number based on X and free-stream conditions, C_f is the skin friction coefficient, based on free-stream conditions and S_t is the Stanton number $q/\rho_\infty U_\infty C_p(T_{0\infty} - T_w)$ where q is the heat transfer to the wall, ρ is the density, C_p is the specific heat at constant pressure, T is the absolute temperature, and the subscripts 0 and w indicate stagnation and wall conditions, respectively. Velocity, stagnation temperature and static temperature profiles are shown at $M = 6$ and 10 for the linearly retarded velocity distribution, cold wall, and two Prandtl numbers.

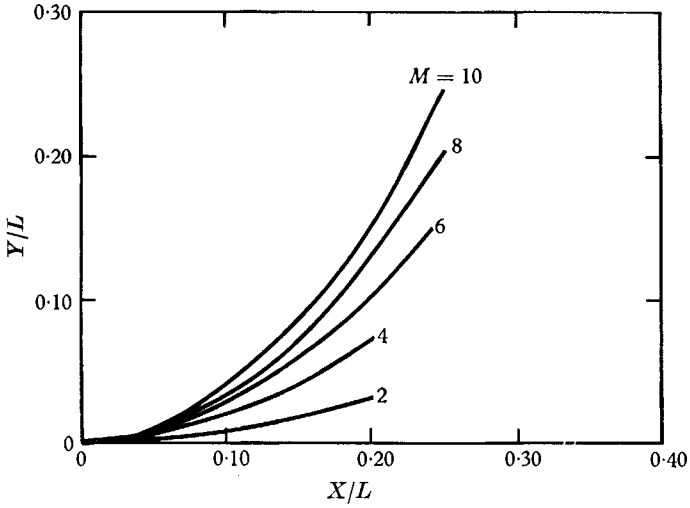

FIGURE 1. Contours which generate a velocity distribution $U_e = U_\infty(1 - X/L)$, for isentropic compression.

3. Adiabatic wall conditions

The recovery factor was assumed to be $\sqrt{P}$, where P is the Prandtl number, and the adiabatic wall temperature is defined by $T_{aw} = T_\infty + \sqrt{P}(U_\infty^2/2C_p)$.

The assumption that the recovery factor is $\sqrt{P}$ is a first approximation near $P = 1{\cdot}0$ and is 'correct' for zero pressure gradient as shown in Stewartson (1964, p. 41). Its validity was tested for adverse pressure gradients by calculating the magnitude of the heat transfer rate in these cases. In this paper solutions labelled **adiabatic wall** imply $T_w = T_R = T_{aw}$ as defined above, where T_R is the recovery temperature, and do not necessarily imply zero heat transfer. Of course, if $P = 1{\cdot}0$ then $T_R = T_{0\infty}$ and the heat transfer is identically zero.

4. Viscosity law assumptions

Although the computer programme can use the Sutherland viscosity law, all calculations except one were made assuming a linear variation of viscosity with temperature. The use of the Sutherland law requires the specification of the

stagnation temperature independently and this is too much of a restriction to put on an otherwise general set of exact solutions. However, in one case ($M = 10$, $T_w = T_\infty$, $P = 0{\cdot}725$ and $T_{0\infty} = 1000\,^\circ\mathrm{K}$) calculations were made using the Sutherland law.

5. Comparisons with other results

The comparisons available are best summarized in a table such as that given below. For details of each individual result, readers are referred to the publication cited.

M	$(X/L)_S$ Present study	$(X/L)_S$ Other studies	
4	0·062	0·062, 0·060, 0·062 0·056, 0·067, 0·066 0·072, 0·064, 0·062 0·061	Morduchow (1965)
		0·054, 0·055	Head & Hayasi (1967)
6	0·043	0·044, 0·042, 0·043 0·037, 0·048, 0·057 0·046	Morduchow (1965)
10	0·026	0·024, 0·023, 0·021 0·023, 0·023	Morduchow (1965)

(*a*) Comparison of results for $P = 1{\cdot}0$, $U_e = U_\infty(1 - X/L)$, adiabatic wall.

M	(X/L_S) Present study	$(X/L)_S$ Other studies	
4	0·204	0·25, 0·173, 0·21, 0·311 0·177, 0·22, 0·227	Morduchow (1965)

(*b*) Comparison of results for $P = 1{\cdot}0$, $U_e = U_\infty(1 - X/L)$, $T_w = T_\infty$.

P	X_S	Other results	
1·0	0·935	0·920	Terrill (1960)†

(*c*) Comparison of results for a cylinder, $U_e = U_\infty(2 \sin X/r)$, $M = 0{\cdot}5$, $T_w = 0{\cdot}5\,T_{0\infty}$, $r = 0{\cdot}5$.

TABLE 1. Comparison of present study with other available results. (Subscript S denotes values at separation point)

It should be noted that our separation points were extrapolated by taking the last three points prior to separation and finding the power n so that C_f was linear in $((X/L)_S - X/L)^n$. It is expected (Morduchow 1965) that n should equal 0·5, provided the separation point and the singular point coincide, but it was found that n was always slightly larger. This effect could be partly due to accumulation of numerical error.

The only exact non-similar solution known to this author prior to this study was the NPL solution for $M = 4$, $T_w = T_\infty$, $P = 1{\cdot}0$ and $U_e = U_\infty(1 - X/L)$. Figure 2 shows this solution compared with our own and three approximate methods.

† Terrill's results for an adiabatic wall.

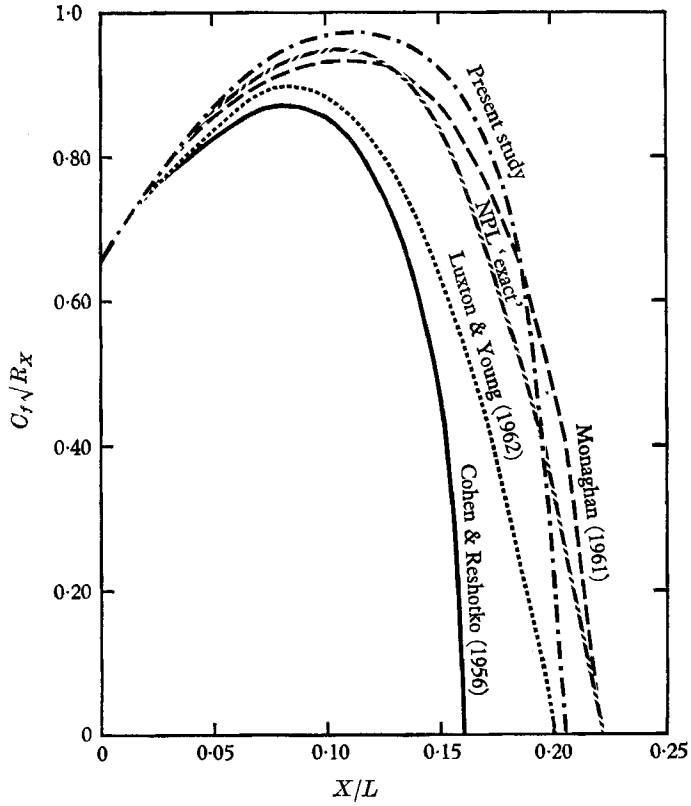

FIGURE 2. Results of present study compared to four other methods. $M = 4$, $T_w = T_\infty$, $P = 1{\cdot}0$, $U_e = U_\infty(1-X/L)$, linear viscosity law.

6. Results from present study

Tables 2–4 list the separation point positions for the cases mentioned previously. Figure 3 shows the variation of $(X/L)_S$ for the linearly retarded velocity distribution and includes unpublished data of Beadle & Sells (as referenced in Cooke & Mangler (1967)) together with the predictions of Gadd (1957) for $P = 1{\cdot}0$. The figure shows that increasing the Prandtl number moves the separation point forward markedly for the case $U_e = U_\infty(1-X/L)$. The percentage shift defined by $1-(X_{1\cdot0}/X_{0\cdot725})_S$ is greater for the hot wall than the cold and increases with Mach number, whereas the percentage shift levels off above $M = 5$ for the cold wall cases. However, in an absolute sense the separation point movement with Prandtl number is much greater in the cold wall cases.

It should be pointed out that it is wrong to conclude that, for an adiabatic wall, increasing the Mach number moves the separation point upstream because in this example of a linearly retarded velocity distribution the body geometry is changing with Mach number.

Gadd (1957) gives an upper limit on $(X/L)_S$ as M tends to infinity and T_w tends to zero. This value was calculated using the Cohen & Reshotko (1956) method

	$T_w = T_R$		$T_w = T_\infty$	
M	$P = 1{\cdot}0$	$P = 0{\cdot}725$	$P = 1{\cdot}0$	$P = 0{\cdot}725$
2	0·091	0·096	0·141	0·143
4	0·062	0·073	0·204	0·232
6	0·043	0·055	0·282	0·325
8	0·029	0·039	0·324	0·372
10	0·026	0·036	0·351	0·405 (0·383)†
11	NC	NC	0·360	NC
12	NC	NC	0·365	NC
13, 14	NC	NC	No separation	NC
15	0·010	NC	No separation	NC

† Sutherland law $T_{0_\infty} = 1000$ °K, $P = 0{\cdot}725$.

TABLE 2. Separation points for $U_e = U_\infty(1 - X/L)$, linear viscosity law.

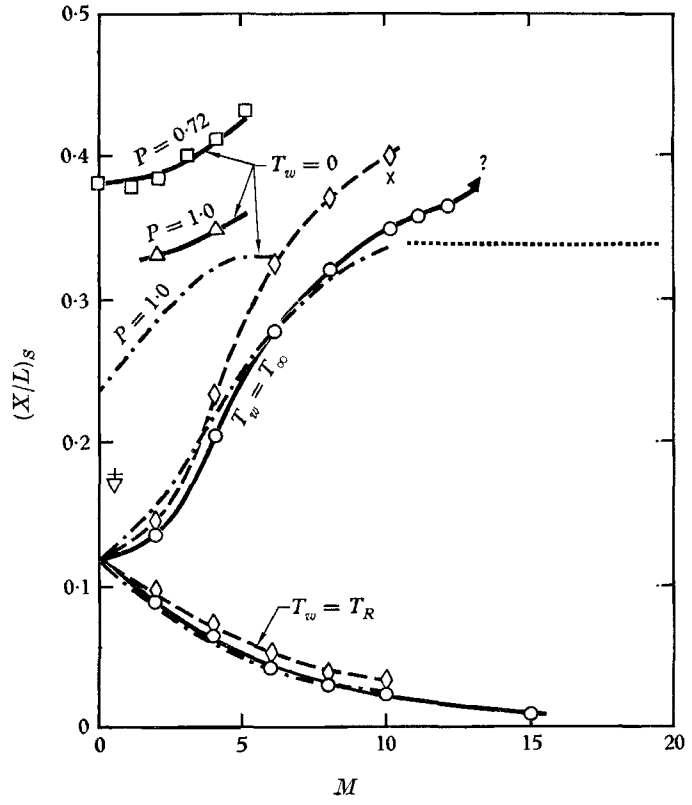

FIGURE 3. Separation points for the linearly retarded velocity distribution. - - - - -, Gadd's asymptotic limit $P = 1{\cdot}0$; ——— ○, $P = 1{\cdot}0$; – – – ◇, $P = 0{\cdot}725$, $U_e = U_\infty(1 - X/L)$, linear viscosity law; — - — - — -, curve of Gadd (1957), $P = 1{\cdot}0$; □, Beadle & Sells, $P = 0{\cdot}72$, $T_w = 0$; △, Sells (1966), $P = 1{\cdot}0$, $T_w = 0$; ×, Sutherland viscosity law, $T_{0_\infty} = 1000$ °K, $T_w = T_\infty$, $P = 0{\cdot}725$; ▽, $M = 0{\cdot}5$, $T_w = 0{\cdot}5T_{0_\infty}$, $P = 1{\cdot}0$; +, $M = 0{\cdot}5$ $T_w = 0{\cdot}5T_{0_\infty}$, $P = 0{\cdot}725$.

However, the results of Beadle & Sells mentioned earlier indicate that for $T_w = 0$, even at low M, $(X/L)_S$ is greater than the value of 0·34 given by Gadd, and the results lie well above Gadd's curve for $T_w = 0$, $P = 1{\cdot}0$.

Calculations with the computer programme at $M = 11, 12, 13, 14, 15$, with $T_w = T_\infty$ and $P = 1{\cdot}0$ show that there was no separation at all above $M = 12$ for the cold wall and the separation points for $M = 11, 12$ are far above the asymptotic limit given by Gadd. At a Mach number of 15, no amount of coaxing could

M	$T_w = 0{\cdot}25T_{0_\infty}$	$T_w = T_R$
2	0·096	0·046
4	Not calculated	Not calculated
6	0·24†	0·072
8	0·27†	Not calculated
10	0·28†	0·080†

† These values accurate only to ± 5 %, due to the step length used.

TABLE 3. Separation points for circular arc, $P = 0{\cdot}725$, linear viscosity law.

	$U_e = U_\infty(1-X/L)$		$U_e = 2U_\infty \sin(X/r)$	
M	$P = 1{\cdot}0$	$P = 0{\cdot}725$	$P = 1{\cdot}0$	$P = 0{\cdot}70$
0·5	0·175	0·178	0·935	0·910
1·1	—	—	0·855	0·851

TABLE 4. Separation points for sinusoidal and linearly retarded velocity distributions. $T_w = 0{\cdot}5T_{0_\infty}$, linear viscosity law.

make the solution separate; C_f would decrease to a very small value and then rise slowly. The locations of the C_f minimum were much further downstream than any of the separation points calculated for lower M. Separation was found for an adiabatic wall and further calculations showed that the boundary layer separated for $T_w = 0{\cdot}5\,T_{0_\infty}$, but no separation was found for $T_w = 0{\cdot}25\,T_{0_\infty}$. Thus it would seem that at a high enough Mach number, sufficient cooling will delay separation indefinitely.

As stated earlier, the programme can calculate with either the Sutherland law or linear viscosity law. The one case run at $T_{0_\infty} = 1000\,°\text{K}$, $M = 10$, $P = 0{\cdot}725$ and $T_w = T_\infty$ is shown in figure 3 and table 2.

Figures 4 and 5 show the non-dimensionalized boundary-layer displacement thickness for the linearly retarded velocity distribution. The effect of Prandtl number can be seen to increase markedly as Mach number increases, and the effect of cooling can be seen by comparing, say, the $M = 10$ curves at the same X/L. The boundary layer is thinned dramatically for $T_w = T_\infty$ reaching one-quarter of its hot-wall thickness. Figure 4 shows that at higher Mach numbers the boundary layer is thinned as it proceeds into an adverse pressure gradient. The Mach number decreases downstream and the local density increase in the boundary layer overrides the entrainment, thus thinning the boundary layer.

Figures 6 and 7 show the distribution of C_f for the linearly retarded velocity distribution for both values of P, and for hot and cold walls. The vast difference

in numerical value of $C_f\sqrt{R_X}$ and the difference in shape of the distribution near the leading edge for the adiabatic wall case are easily discernible. The reader is reminded of the great difference in scale between figure 6 and figure 7.

Figure 8 shows the variation of Stanton number for the linearly retarded velocity distribution. The curves show qualitatively the same behaviour as the

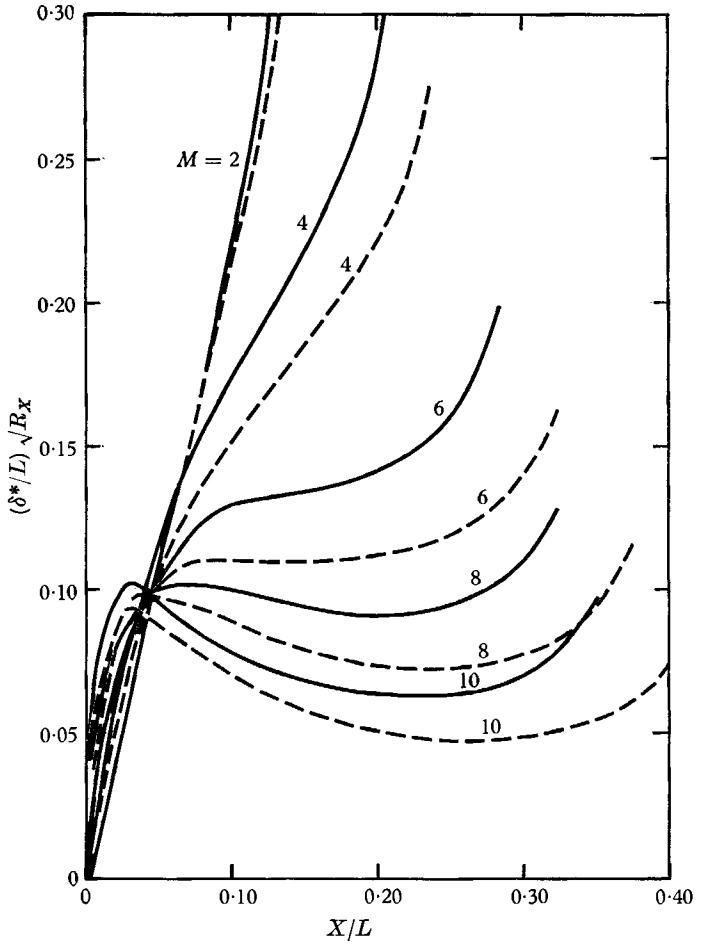

FIGURE 4. Displacement thickness for the linearly retarded velocity distribution, cold wall. $U_e = U_\infty(1-X/L)$, $T_w = T_\infty$, linear viscosity law. ———, $P = 1{\cdot}0$; — — —, $P = 0{\cdot}725$.

corresponding trends in C_f (figure 6) but S_t never approaches zero and inspection of figures 6 and 8 together show that C_f/S_t starts at 2·0 (for $P = 1{\cdot}0$) at $X/L = 0$ and proceeds smoothly to zero at separation.

The linearly retarded velocity distribution is a continuously adverse pressure gradient. It was thought worthwhile to compare its trends with those of a pressure gradient which is initially favourable but later turns adverse. For the latter case, the velocity distribution $U_e = 2U_\infty \sin X/r$ was chosen, and $r = 0{\cdot}5$. Figure 9

shows the variation in C_f, δ^* and S_t for the cylinder at Mach number 0·5, where r is the radius of the circular arc body.

For the linearly retarded velocity distribution, a higher Prandtl number leads to lower Stanton numbers, lower skin friction, higher values of displacement thickness and earlier separation. For the sinusoidal velocity distribution it was

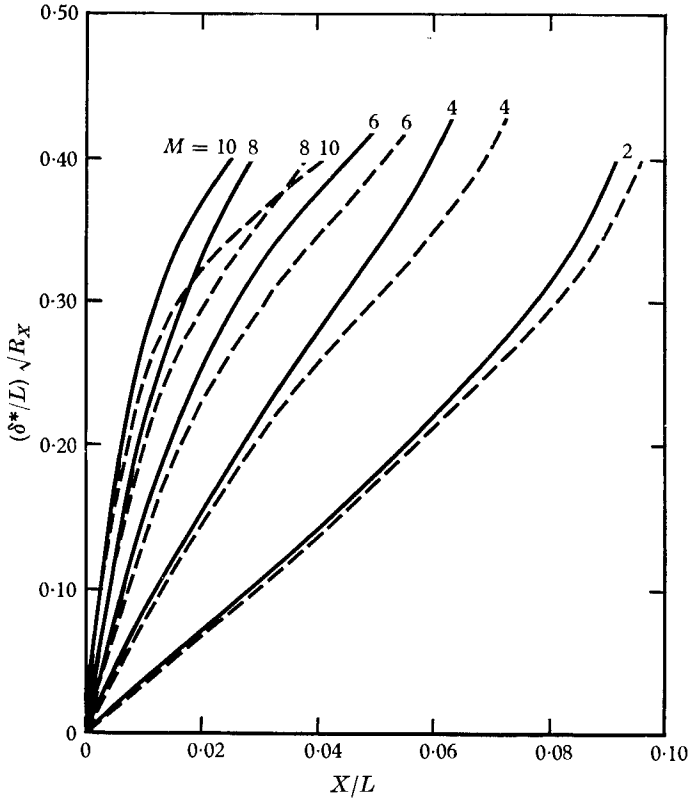

FIGURE 5. Displacement thickness for the linear retarded velocity distribution, adiabatic wall. $U_e = U_\infty(1-X/L)$, $T_w = T_R$, linear viscosity law. ———, $P = 1{\cdot}0$; — — —, $P = 0{\cdot}725$.

found that a higher Prandtl number led to lower Stanton numbers, higher values of displacement thickness, higher skin friction and later separation. This partial reversal of trends must be due to the difference in pressure gradient and to the fact that one flow begins from a sharp leading edge while the other is a stagnation point flow. Both types of pressure gradient were calculated at subsonic and supersonic Mach numbers, and the trends for each flow were the same for both subsonic and supersonic free streams, although the supersonic sinusoidal velocity distribution is no longer the flow over a cylinder.

Figures 10 and 11 show at $M = 6$, 10 respectively, the velocity, stagnation temperature and static temperature profiles across the boundary layer for Prandtl numbers of 1·0 and 0·725. In these graphs, separation refers to the last profile calculated by the programme; the actual separation point is slightly

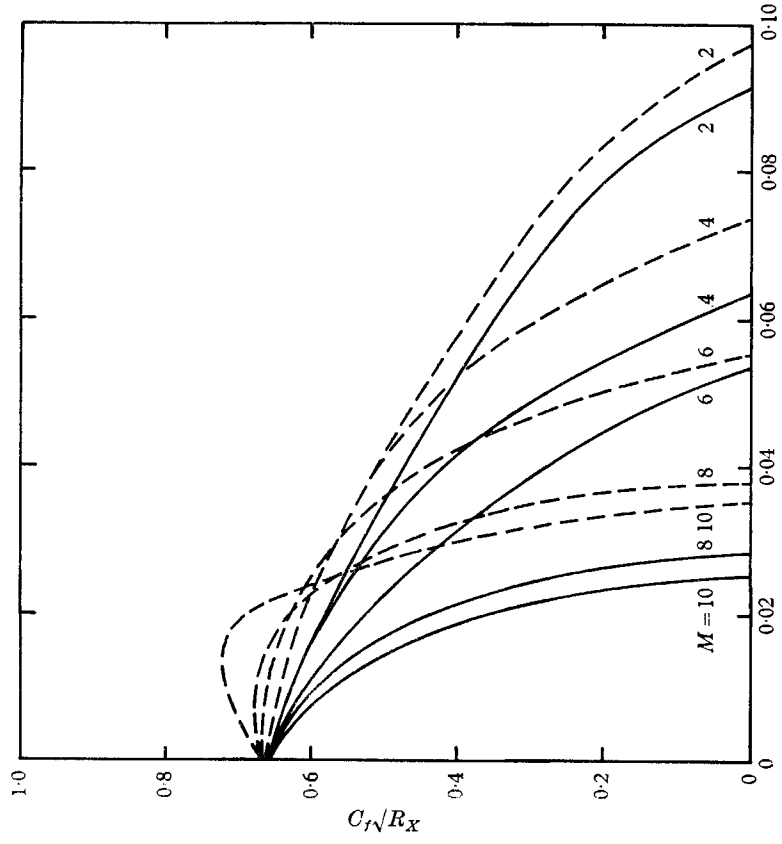

FIGURE 7. Skin friction for the linearly retarded velocity distribution, adiabatic wall. $U_e = U_\infty(1-X/L)$, $T_w = T_R$, linear viscosity law. ———, $P = 1{\cdot}0$; — — —, $P = 0{\cdot}725$.

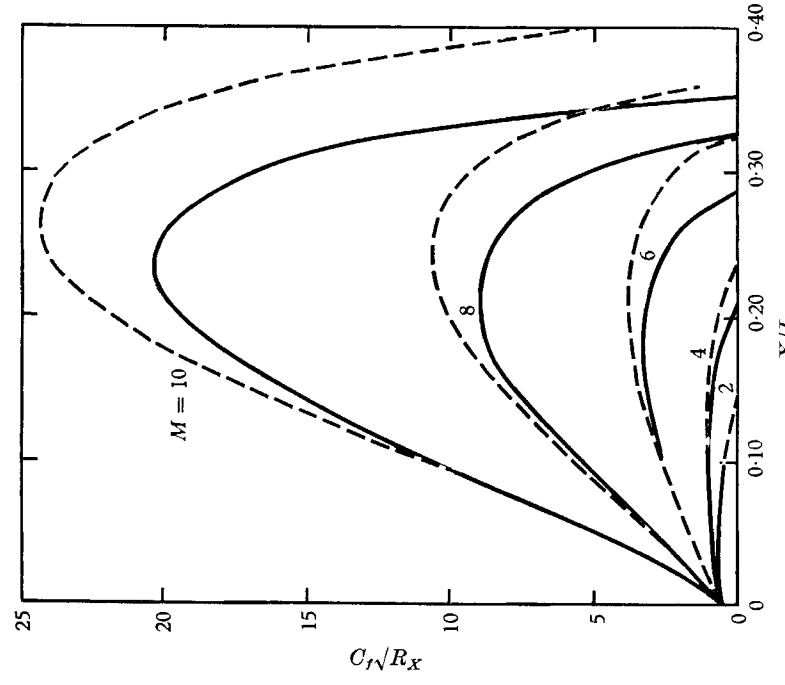

FIGURE 6. Skin friction for the linearly retarded velocity distribution, cold wall. $U_e = U_\infty(1-X/L)$, $T_w = T_\infty$, linear viscosity law. ———, $P = 1{\cdot}0$; — — —, $P = 0{\cdot}725$.

further downstream. The effect of P is marked, especially on the static temperature. It should be noted when the velocity gradient at the wall approaches zero, the stagnation and static temperature gradient is still non-zero. Near separation, the curves at each P for equal values of X/L cease to coincide at all, because one flow is much nearer separation than the other.

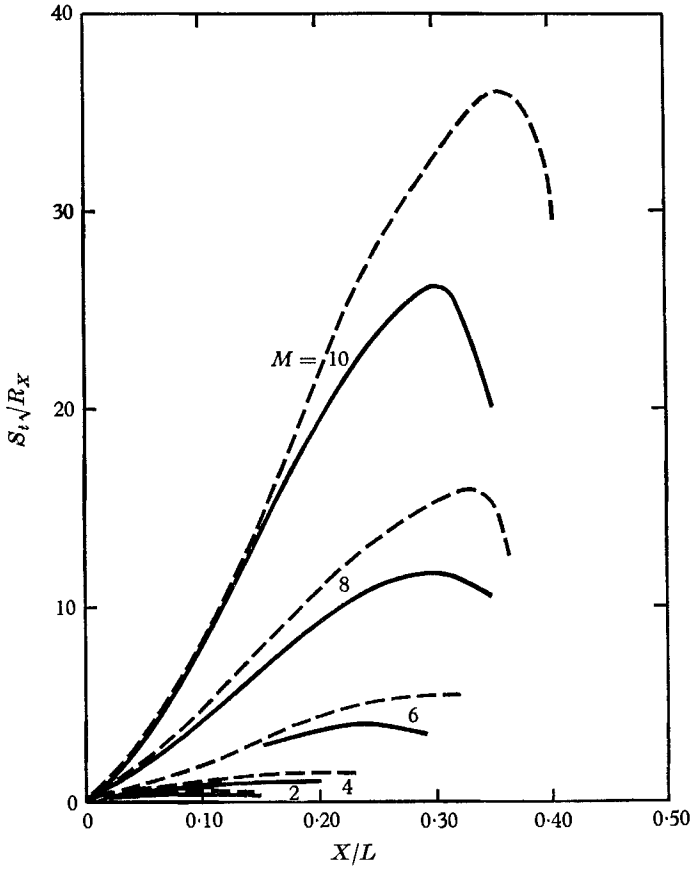

FIGURE 8. Heat transfer for the linearly retarded velocity distribution. $U_e = U_\infty(1-X/L)$, $T_w = T_\infty$, linear viscosity law. ———, $P = 1{\cdot}0$; — — —, $P = 0{\cdot}725$.

Figure 12 shows the separation points on the circular arc for cold and adiabatic walls. The separation point is very insensitive to Mach number for the adiabatic cases, but moves rearward as M increases for the cold wall case. The value of this study is that the circular arc is of constant geometry unlike the $U_e = U_\infty(1-X/L)$ distribution and shows that at constant Mach number, cooling the wall delays separation. Figures 13–15 show the variation in δ^*, C_f and S_t for the circular arc. Again dramatic thinning of the boundary layer with cooling can be seen in figure 13, where the difference between hot and cold wall displacement thickness can be as much as a factor of 3. The marked thinning of the boundary layer as it proceeds downstream in the cold wall cases is also evident. The curves for C_f and S_t show again that S_t does not approach zero as C_f does.

Flows at the same Mach number, each near separation (different X/L, therefore), were compared and it was seen that at high Mach numbers the 'adiabatic' wall sustained much less heat transfer, compared to the case where $T_w = T_\infty$, than did flows at low Mach numbers. At Mach number 2, the 'adiabatic' Stanton number was 30 % of its cold wall counterpart, but at higher Mach numbers, the figure was progressively reduced until at $M = 10$, the heat transfer was 3 % of

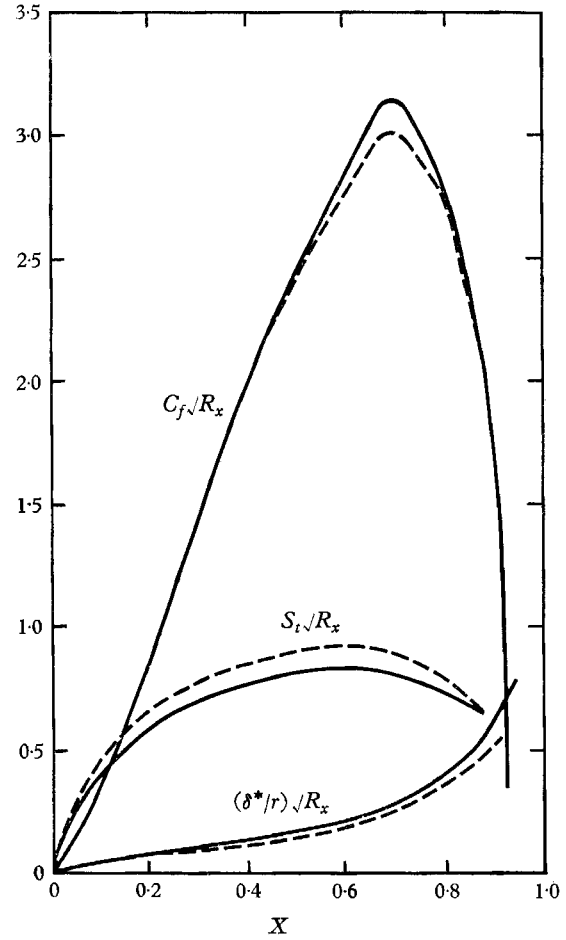

FIGURE 9. Displacement thickness, skin friction and heat transfer for a cooled cylinder. $M = 0{\cdot}5$, $T_w = 0{\cdot}5T_{0_\infty}$, $U_e = 2U_\infty \sin X/r$, linear viscosity law. ———, $P = 1{\cdot}0$; — — —, $P = 0{\cdot}70$, $r = 0{\cdot}5$.

its cold wall counterpart. This trend was also found on the circular arc and we conclude that assuming that the recovery factor is equal to P is a better assumption at high Mach numbers than at low ones. It should be noted that these conclusions are drawn from considerations of $S_t\sqrt{R_X}$, not from S_t alone. It is worth remarking that Clutter & Smith (1963) have found the same trend on a flat plate and a cone, also assuming a linear viscosity law. Their calculations show that the recovery factor approaches $\sqrt{P}$ and becomes identical to it at $M = 9$.

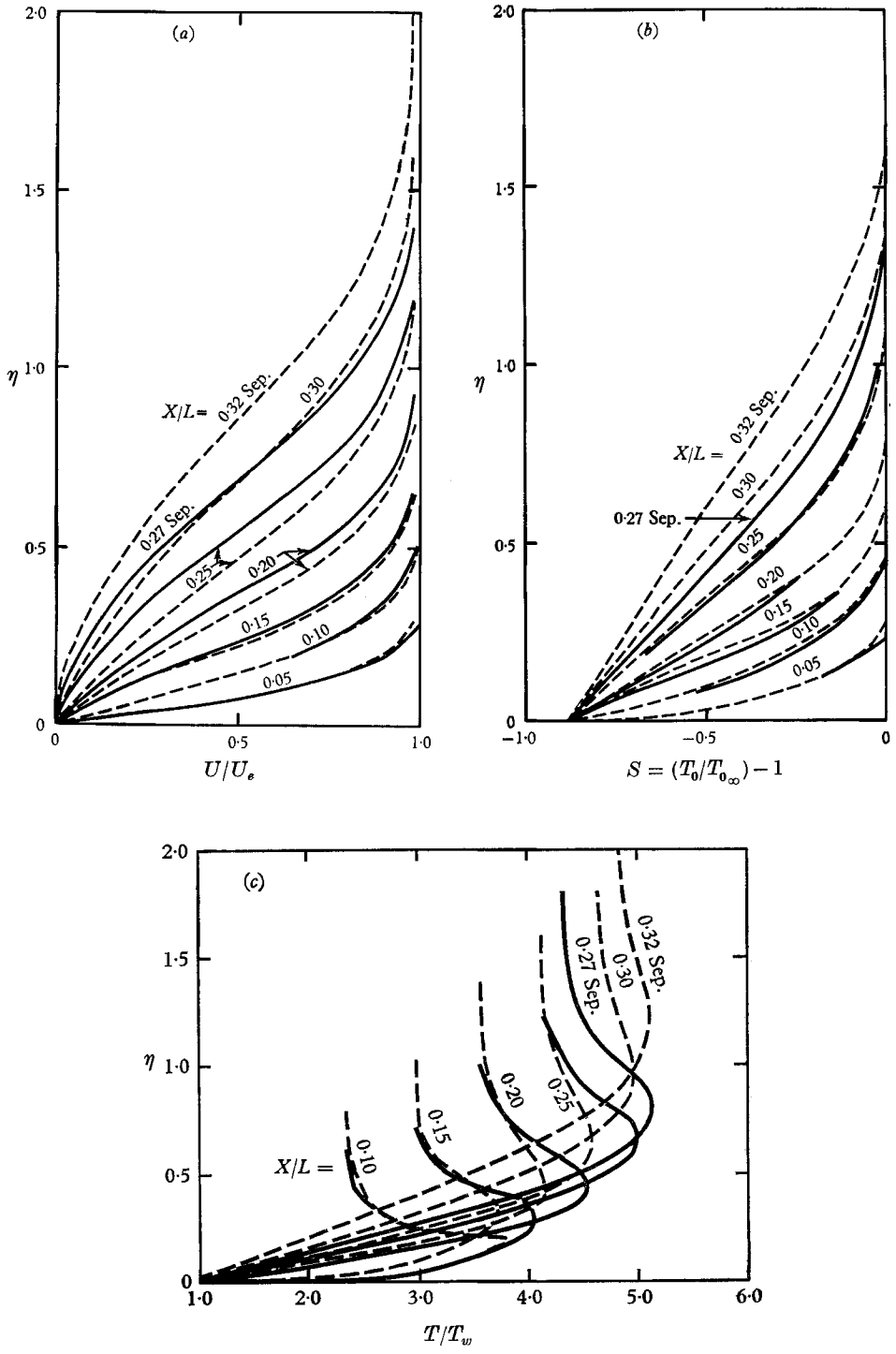

FIGURE 10. Velocity, stagnation and static temperature profiles for the linearly retarded velocity distribution. $M = 6$, $T_w = T_\infty$, $U_e = U_\infty(1 - X/L)$, linear viscosity law. ———, $P = 1{\cdot}0$; — — —, $P = 0{\cdot}725$.

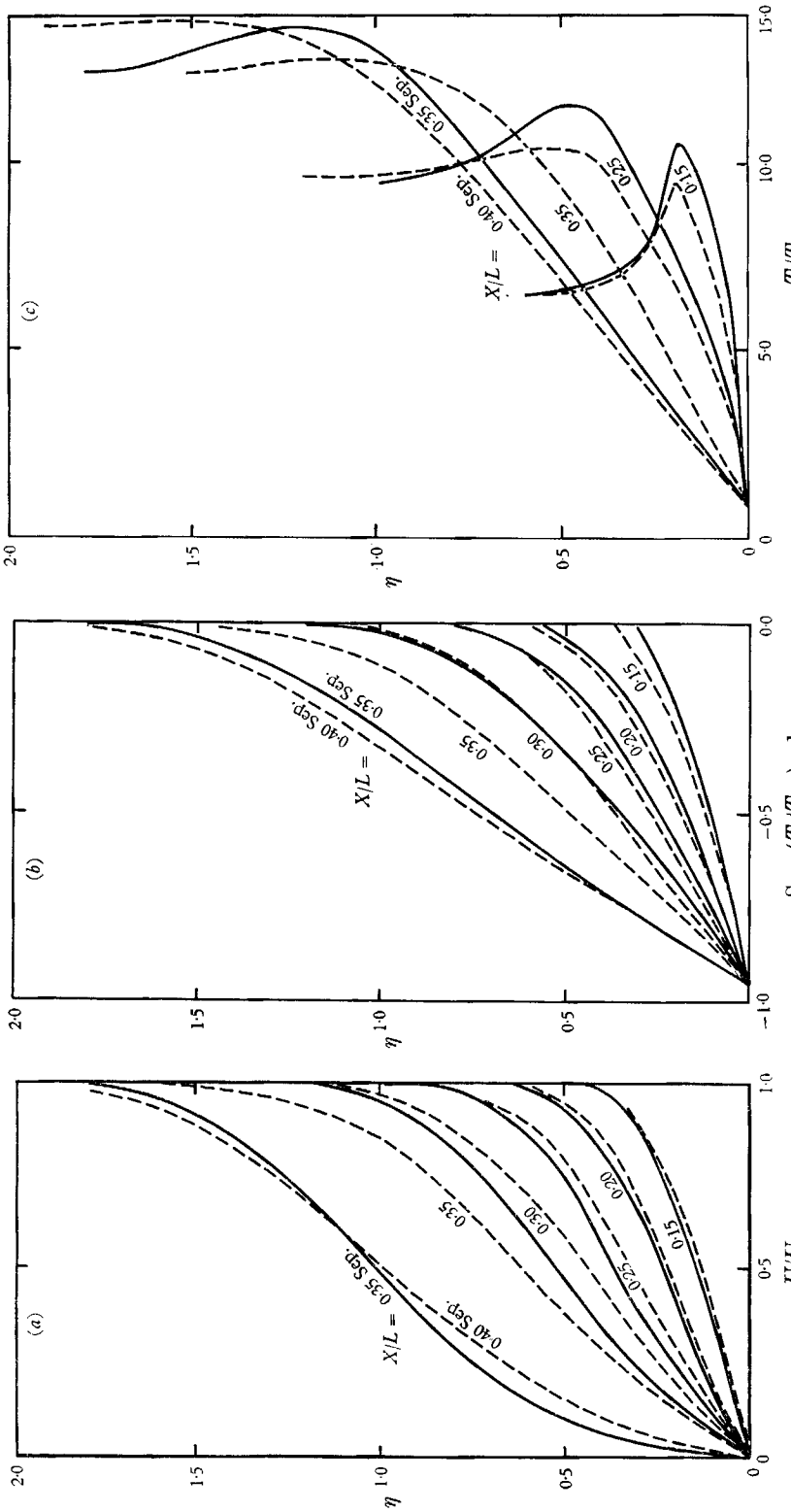

FIGURE 11. Velocity, stagnation and static temperature profiles for the linearly retarded velocity distribution $M = 10$. $U_e = U_\infty(1 - X/L)$, $T_w = T_\infty$. ———, $P = 1{\cdot}0$; — — —, $P = 0{\cdot}725$.

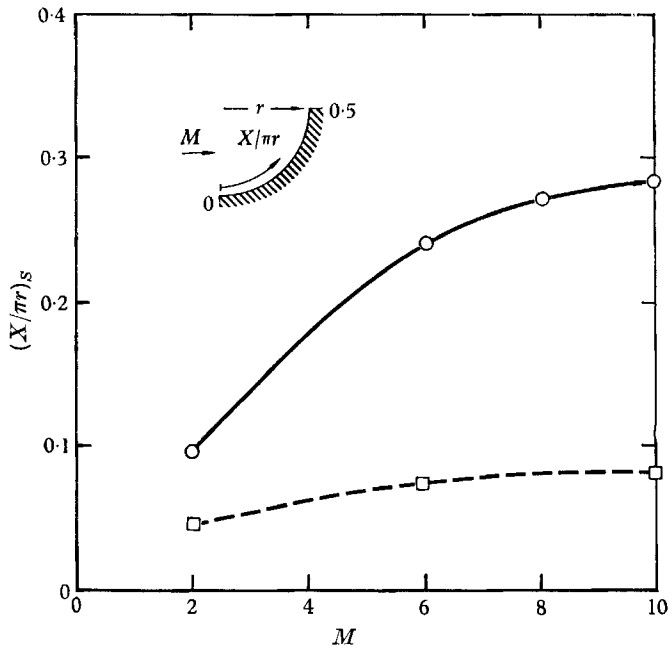

FIGURE 12. Separation points on a circular arc for adiabatic and cold walls. $P = 0{\cdot}725$, linear viscosity law. ——— ○, $T_w = 0{\cdot}25T_{0_\infty}$; — — — □, $T_w = T_R$.

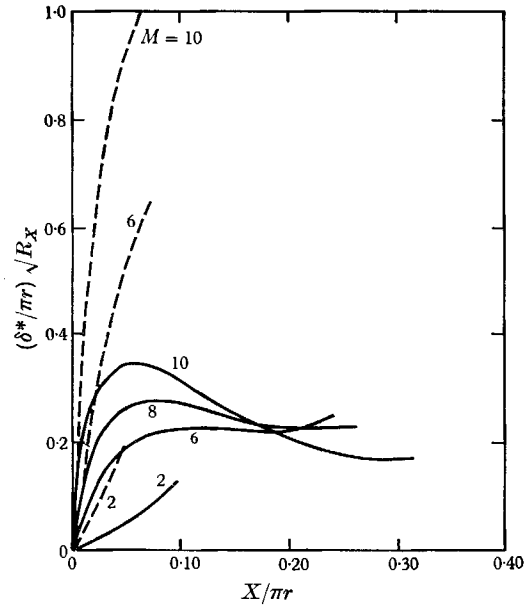

FIGURE 13. Displacement thickness on the circular arc for adiabatic and cold walls. $P = 0{\cdot}725$, linear viscosity law. ———, $T_w = 0{\cdot}25T_{0_\infty}$; — — —, $T_w = T_R$.

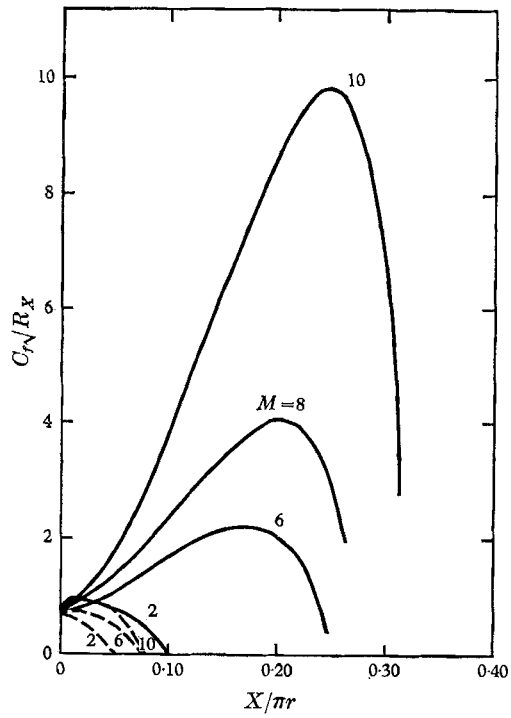

FIGURE 14. Skin friction on the circular arc for adiabatic and cold walls. $P = 0{\cdot}725$, linear viscosity law. ———, $T_w = 0{\cdot}25T_{0_\infty}$; — — —, $T_w = T_R$.

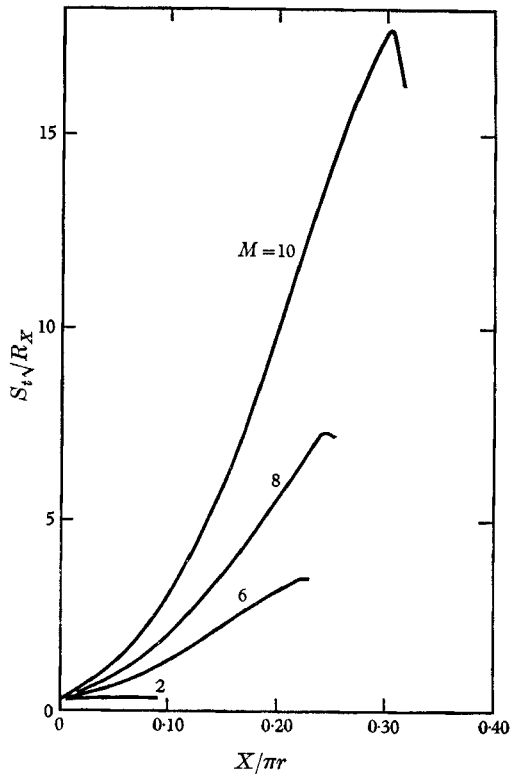

FIGURE 15. Heat transfer on the circular arc. $P = 0{\cdot}725$, $T_w = 0{\cdot}25T_{0_\infty}$, linear viscosity law.

Figures 6, 8, 9, 14 and 15 show that the skin friction maximum does not occur at the same point as the heat transfer maximum, thus discrediting the often-made assumption that heat transfer and skin friction behave similarly, although not necessarily in accord with Reynolds's analogy. Far more important, however, is the fact that the heat transfer is definitely not zero at the separation point. Inspection of figures 8, 9 and 15 shows that $S_t\sqrt{R_X}$ cannot logically be extrapolated to zero at the same point as $C_f\sqrt{R_X}$ can. Moreover, on the occasions when the computer programme managed to converge beyond separation, the heat transfer was definitely positive and only slightly reduced from its separation point value, even though C_f was negative.

7. A comparison of Monaghan's correlation method with present results

Monaghan (1961) has published the last in a series of correlation techniques which drew upon the analysis of Cohen & Reshotko (1956) and others. His method depends on the correlation of separation point locations from exact solutions. His correlation parameter is defined as

$$m = -0{\cdot}44\frac{T_w}{T_e}\frac{\bar{X}}{U_e}\frac{dU_e}{d\bar{X}},$$

where

$$\bar{X} = \int_0^X \left(\frac{T_e}{T_w}\right)^4 M_e^g\, dX \Big/ \left(\frac{T_e}{T_w}\right)^4 M_e^g$$

and

$$g = 3 + 2T_w/T_{0\infty}.$$

Monaghan found for adiabatic wall conditions and $P = 1{\cdot}0$ that $m_S = 0{\cdot}0681$ when correlated from the similar solutions of Cohen & Reshotko (1956), and $m_S = 0{\cdot}084$ for Thwaites's correlations of incompressible solutions for the case of a linearly retarded velocity distribution. (Readers are referred to § 6.2 of Monaghan (1961).) Further correlation produced a curve from which m_S for flows with heat transfer could be determined from the adiabatic wall value of m_S. Thus, knowing m_S, and integrating the above equations to yield $m(X)$, it is possible to determine the separation point for any arbitrary adverse pressure gradient.

Knowing the exact separation point for a number of cases where

$$U_e = U_\infty(1 - X/L),$$

we can find the values of m_S at these points and compare them with the values of m_S predicted by Monaghan's method. This comparison is summarized in tables 5 and 6, which contain in the first three columns the Mach number, separation point location and value of m_S predicted by the current study. The other two columns show the value of m_S taken by Monaghan assuming that m_S (adiabatic) is 0·0681 and 0·084 respectively.

From table 5(*a*) it can be seen that Monaghan's values of m_S for adiabatic walls and linear velocity distributions are correct to within 4 %, but table 5(*b*) shows poorer agreement for cold walls, where errors vary between 0 and 12 %.

M	$(X/L)_S$	m_S	m_S correlation of similar solutions	m_S Thwaites's correlation
0	0·120	0·0846	0·0681	0·084
2	0·091	0·0811	0·0681	0·084
4	0·062	0·0826	0·0681	0·084
6	0·043	0·0821	0·0681	0·084

(*a*) $P = 1{\cdot}0$, adiabatic wall.

M	$(X/L)_S$	m_S	m_S correlation of similar solutions	m_S Thwaites's correlation
0·5†	0·175	0·0723	0·051	0·063
2	0·141	0·0693	0·055	0·067
4	0·204	0·0387	0·034	0·042
6	0·282	0·0248	0·0204	0·025

(*b*) $P = 1{\cdot}0$, $T_w = T_\infty$, except where † indicates $T_w = 0{\cdot}5T_{0_\infty}$.

TABLE 5. Values of m_S at exact separation points of present study. $P = 1{\cdot}0$, $U_e = U_\infty(1 - X/L)$. Linear viscosity law.

M	$(X/\pi r)_S$	m_S	m_S correlation of similar solutions	m_S Thwaites's correlation
2	0·046	0·079	0·0681	0·084
6	0·072	0·076	0·066	0·082
10	0·080	0·087	0·065	0·080

(*a*) $T_w = T_R$.

M	$(X/\pi r)_S$	m_S	m_S correlation of similar solutions	m_S Thwaites's correlation
2	0·096	0·055	0·034	0·042
6	0·24	0·043	0·034	0·042
10	0·28	0·036	0·034	0·042

(*b*) $T_w = 0{\cdot}25T_{0_\infty}$.

TABLE 6. Values of m_S at separation points of present study for a circular arc. $P = 0{\cdot}725$. Linear viscosity law.

Table 6(*a*) shows reasonable agreement between the exact values of m_S for flow on a circular arc and the values from the correlation of the linear velocity distribution, for an adiabatic wall. Table 6(*b*) shows poor agreement of m_S with either value of m_S predicted by Monaghan's method.

From the above results, it would appear that Monaghan's method is reliable only if a suitable correlation exists for the problem to be studied. For an arbitrary problem such correlations are seldom available and for that reason the method cannot be relied upon. In passing, it should be pointed out that if $T_w = 0$, then Monaghan's method predicts $m(X) = 0$, and there is no separation at all, contrary to the results of Beadle & Sells.

8. Conclusions

Increasing Prandtl number leads to earlier separation in an adverse pressure gradient given by $U_e = U_\infty(1 - X/L)$, but this trend is reversed for a favourable pressure gradient which turns adverse as specified by $U_e = U_\infty(2 \sin X/r)$. The percentage shift is greater for a hot wall than for a cold wall. For both types of pressure gradient, a higher Prandtl number leads to lower heat transfer and greater displacement thickness.

At constant Mach number, wall cooling delays separation for the adverse pressure gradient and at constant wall temperature increasing Mach number delays separation, although the latter effect is small for an adiabatic wall. For the favourable pressure gradient which later turns adverse, increasing the Mach number causes earlier separation at constant (cold wall) temperature.

Using the linear viscosity–temperature relation instead of the Sutherland viscosity law has a small effect on separation point location.

Strong cooling has an enormous effect on skin friction and displacement thickness, the former being increased by a factor of 20 and the latter being reduced by a factor of 3 (see § 6).

The heat transfer for a cold wall is non-zero at the separation point, where C_f/S_t proceeds smoothly to zero.

The assumption that the recovery factor is $\sqrt{P}$ is better at high Mach numbers than at low ones.

Changing the Prandtl numbers has a great effect on the static temperature profile and on the velocity and stagnation temperature profile near separation.

If the free stream Mach number is high enough ($M \gtrsim 5$), the boundary layer is thinned as it proceeds into a strong adverse pressure gradient.

Concluding remarks

As stated previously, all of the results of this paper are first-order solutions to the boundary layer equations and the question of the importance of second-order effects naturally arises. Lewis (1967) and Adams (1967), for example, have shown that in some hypersonic cases, second-order effects can contribute more skin friction than the first-order solution. The results given in this paper are accurate solutions to the first-order problem, but are only intended to give qualitative conclusions concerning the behaviour of the hypersonic laminar boundary layer.

Special thanks are due to the author's supervisor, Mr J. L. Stollery, for his valuable inspiration, criticism and moral support in the course of this work; thanks are also due to Dr C. C. L. Sells for providing a copy of his computer programme, and for subsequent helpful discussions.

Parts of this paper were originally reported as AGARD Conference Proceedings, May 1968.

REFERENCES

ADAMS, J. C. 1967 Higher order boundary layer effects on analytic bodies of revolution. *ARO, Inc. Arnold Air Force Station, Tennessee.*

CLUTTER, D. W. & Smith, A. M. O. 1963 Solutions of the general boundary layer equations for compressible laminar flow, including transverse curvature. *Douglas Aircraft Co.* Dept. LB 31088.

COHEN, C. B. & RESHOTKO, E. 1956 The compressible laminar boundary layer with heat transfer and arbitrary pressure gradient. *NACA Rep.* 1294.

COOKE, J. C. & MANGLER, K. W. 1967 The numerical solution of the laminar boundary layer equations for an ideal gas in two and three dimensions. *RAE Tech. Memo* AERO 999.

GADD, G. E. 1957 A review of theoretical work relevant to the problem of heat transfer effects on laminar separation *ARC* CP 331.

HEAD, M. R. & HAYASI, N. 1967 Approximate calculation of the incompressible laminar boundary layer. *Aero. Quarterly*, **18**, 259.

LEWIS, C. H. 1967 First- and second-order boundary layer effects at hypersonic conditions. *ARO, Inc. Arnold Air Force Station, Tennessee.*

LUXTON, R. E. & YOUNG, A. D. 1962 Generalised methods for calculation of the laminar compressible boundary layer characteristics with heat transfer and non-uniform pressure distribution. *Aero Res. Counc. R. & M.* no. 3233.

MONAGHAN, R. J. 1961 Effects of heat transfer on laminar boundary layer development under pressure gradients in compressible flow. *Aero. Res. Counc. R. & M.* no. 3218.

MORDUCHOW, M. 1965 Review of theoretical investigations on effect of heat transfer on laminar separation. *AIAA J.* **3**, 1377.

SELLS, C. C. L. 1966 Two-dimensional laminar compressible boundary layer programme for a perfect gas. *RAE TR* 66243.

STEWARTSON, K. 1964 *The Theory of Laminar Boundary Layers in Compressible Fluids.* Oxford: Clarendon.

TERRILL, R. M. 1960 Laminar boundary layer flow near separation with and without suction. *Phil. Trans.* A **253**, 55.